NONLINEAR MATHEMATICAL MODEL OF HELICOPTER MOTION

V.A.Leontiev, V.A.Anikin (Russia)
Central Aerohydrodynamic Institute (TsAGI), KAMOV Company

A universal mathematical model of rotocraft dynamics is considered. The model makes it possible to simulate:

- operational conditions of flight (takeoff, landing, steady and transient modes, maneuvering, ground run);
- special regimes of flight (vortex ring, ground proximity);
- flight with the failure of major functional systems and beyond the flight restrictions.

The structure and the degree of detailing of the mathematical model are defined by demands for its practical implementation.

When studying safe operation of the vehicle in conditions of dangerous loading of the structural components, inadmissible closing of the blades with the structure, entry into regimes with poor controllability, etc., most sophisticated mathematical models are required which would enable computations with a consideration of stall, compressibility, elastic deformations. In solving the other problems there is no need of applying such complicated models and the computation can be carried out, for example, with or without considering for elastic deformations.

Taking into account the variety of problems under study, TsAGI together with design bureaux has developed a modular structure of a mathematical model which makes it possible to generate the model of a required level of complexity by replacing separate modules. The mathematical model is based on a full system of nonlinear differential equations of helicopter motion, incorporating the equations of its center of masses motion and the equations of helicopter rotation about the center of masses, kinematic equations of coupling of angles and rates of pitch, roll and yaw, as well as the equations of trajectory for center of masses motion in space (Fig.1).

In a general case the mathematical model incorporates two main rotors, a fuselage, a wing with flaps and ailerons, movable stabilizer, two fins with rudders and different variants of devices for directional control (tail rotor, jet system or fenestron). The mathematical models of a powerplant, automatic control system and undercarriage can be introduced additionally (Fig.2).

Such an approach makes it possible to configure the models of single-rotor and twin-rotor (co-axial, longitudinal, lateral) layouts with different degree of detailing in each particular case.

At first, let us briefly examine the operation of the modules typical of all mathematical models under consideration.

The aerodynamic characteristics of the airframe components (fuselage, wing, stabilizer and fin) are determined by using the results of the wind-tunnel tests with due regard for the effect of the main rotor, and, if necessary, with accounting for ground proximity (Fig.3).

When determining the aerodynamic characteristics of the tail rotor and airframe components (wing, horizontal and vertical tails), it is necessary to take into account the influence of the main rotors on them. For this purpose the velocities induced by each main rotor are computed at certain points of structural components. The sum of these velocities is considered for in deriving the aerodynamic characteristics of wing, empennage and tail rotor (Fig.4). In order to determine the induced velocities due to the main rotors at an arbitrary point of space a quasilinear disk vortex theory using a computational scheme of the skewed vortex cylinder is applied [1,2]. In this case the expansion of the induced velocity components into a Fourier series is used. For the expansion coefficients the formulae are derived in which analytical peculiarities relating to the computation of the velocities inside the vortex cylinder are singled out.

A consideration of air flow deceleration due to the main rotor hub is a special feature of the computational scheme for the induced velocities (Fig.5). Behind the hub, in the vicinity of the vortex cylinder axis, a deceleration zone is selected. Its size and the value of the deceleration coefficient are obtained on the basis of experimental data.

The change of the frequency of the main rotor rotation is accounted for by simulating static and dynamic characteristics of the engine running together with the transmission and autothrottle system. The control deflections are determined by moving the control levers with accounting for the operation of the automatic control system and actuator limitations.

The rotor forces and moments are determined by summing up elementary forces and moments acting at the blade sections with using the data of wind tunnel tests of aerodynamic airfoils. The blade motion is simulated with accounting for the elastic deformations in the planes of thrust, rotation and torsion and with due regard for the an elastic

coupling among the blades across the swashplates.

The paper presents the equations of the blade motion given in the form of conditions of equilibrium of the distributed forces and torque moments over the blade element for a general case of helicopter motion (Fig.6).

A weightless elastic beam divided into 20 segments with bending and torsional stiffnesses constant at each segment and masses localized on segment boundaries is considered as a computed blade model (Figs.7-8).

Time-average induced velocities are obtained on the basis of the quasiliniar vortex disc theory using the computational scheme of the skewed vortex cylinder. A nonstationary flow past the blade at substall angles of attack is taken into consideration on the base of the linear nonstationary theory of the blade section. A semiempirical method is used to account for an oscillating airfoil separation delay.

The motion of all blades is determined by solving a similar system of equations with corresponding variation of exciting loads and boundary conditions. This system represents a set of differential equations written in partial derivatives of the fourth order. To transform this system into a system of ordinary differential equations the Galerkin method is used.

The movements of a blade in the flap and lag planes are set in the form of decomposition of the deformations by the shapes of natural blade oscillations. With the aim of a more exact accounting for the effect of the control system distortion and the friction in the feathering hinge, the torsional deformations are set as the sum of non-orthogonal functions.

For a numerical integration of the above system a special combined method is used where the solution at two first points is found by the Runge-Kutta method of the fourth order. Then, the solution is searched for by using a multistep method for prediction and correction. In the case under consideration the combined method provides the best results (Fig.9).

RESULTS OF SIMULATION

In three-dimentional helicopter motion the mathematical model makes it possible to define:

- momentary and mean, distributed and total forces and moments acting upon lifting and structural components (blades and hubs of rotors, swashplate and hydraulic actuator rods, fuselage, empennage, wing, undercarriage legs);
- flapping motion in thrust and lag planes, elastic deformations and hinge moments, dynamic stress state of the rotor blades;
- coefficients of linear equations of helicopter motion;
- longitudinal and lateral trim characteristics;
- response characteristics of three-dimensional controlled motion of helicopter.

Figure 10 illustrates the comparison of the results of computing the total forces and moments of a full-scale main rotor with the wind tunnel test data obtained for different flight conditions (Fig.11). A satisfactory agreement of computed and experimental values is shown.

Computed aeroelastic characteristics of the main rotor blades and their comparison with flight-test data are given, as an example, in Figs.12-14. Figure 12 illustrates the amplitudes of alternate bending stresses in the flapping plane and the variation of these stresses against the azimuthal angle of the upper rotor blade of the co-axial helicopter for different conditions of horizontal steady flight. The change in alternate and constant parts of the main rotor blade hinge moment of the single-rotor helicopter when flying turns with different value of the load factor is given in Fig.13. Figure 14 illustrates the comparison of computed and experimental values for the alternate and constant parts of the main rotor hinge moment of the single-rotor helicopter in performing steep climb.

In Fig.15 compared are the computed values of the swashplate longitudinal and lateral deflection angles, the values of the main rotor collective pitch and tail-rotor pitch, roll and pitch angles of the single-rotor helicopter in trimmed level flight (with various values of the longitudinal c.g.position) with similar flight-test data.

Experimental and computed trim values of the main collective pitch, tail-rotor pitch and roll angle of the single-rotor helicopter in climb conditions, autorotation descent and level flight are compared in Fig.16.

The examples of comparing the computed dependences between roll angles and the slip angle for different speeds of level flight with those obtained in flight tests are shown in Fig.17. In the same figure compared are the computed values of the vertical velocities of descent in autorotation and maximum rate of climb of the single-rotor helicopter with the flight-test data.

A comparison between the computed values of the swashplate longitudinal deflection and pitch angles in trimmed level flight of the co-axial helicopter (with different values of longitudinal c.g.position) and similar data of flight tests is presented in Fig.18. Here is also shown a correlation between the values of directional control in sideward flight.

Fig.19 illustrates the comparison of computed and experimental closing of the blades for the upper and lower rotors.

In Figures 20-22 shown is a comparison between computed parameters of dynamic response to standard control actions of single-

rotor helicopter in level flight with speed of 180 km/hour and corresponding flight-test data. Figure 20 presents directional control input, Fig.21 - lateral control input, Fig.22 - longitudinal control input.

For a number of years the above models have been effectively applied in solving a wide range of practical tasks.

REFERENCES

1.В. .Баскин, Л.С.Вильдгрубе, Е.С.Вождаев, Г.И.Маикопар. Теория несущего винта.-М.: Машиностроение, 1973.

2.В.А.Аникин, В.А.Леонтьев. асчет а роупругих характеристик соосных несущих винтов при пространственном движении вертолета.-М., МАИ, 1983.

3.В.А.Аникин. Дисковая вихревая теория винта и ее приложение в а родинамике вертолетов.- Труды вторых научных чтении, посвященных памяти Б.Н.Юрьева. Москва, март 1987, ИИЕ АН ССС , М., 1988.

NONLINEAR MATHEMATICAL MODEL OF HELICOPTER MOTION

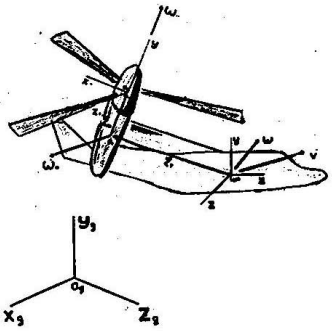

$$m\left(\frac{d\vec{V}_к}{dt} + \vec{\omega} \times \vec{V}_к\right) = \vec{R} + \vec{F}_{гр};$$

$$\frac{d\vec{K}}{dt} = \vec{M}_R;$$

$$J_\omega \frac{d\vec{\omega}_н}{dt} = \vec{M}_{дв} + \vec{M}_{пр};$$

$$\vec{R} = \sum_1^2 \vec{R}_{кв} + \vec{R}_ф + \vec{R}_{кр} + \vec{R}_{во} + \vec{R}_{го} + \vec{R}_р;$$

$$\vec{M}_R = \sum_1^2 \vec{M}_{кв} + \vec{M}_ф + \vec{M}_{кр} + \vec{M}_{во} + \vec{M}_{го} + \vec{M}_р;$$

$$\frac{dx}{dt} = F(x, u, f); \quad u = u(\delta_{пр}, \delta_{по}, \delta_н, \delta_{пз}, \varphi_д)$$

Fig. 1

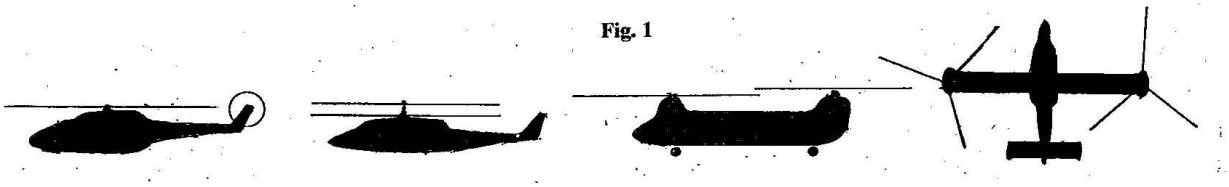

Diagram for interacting the elements of helicopter flight dynamics block

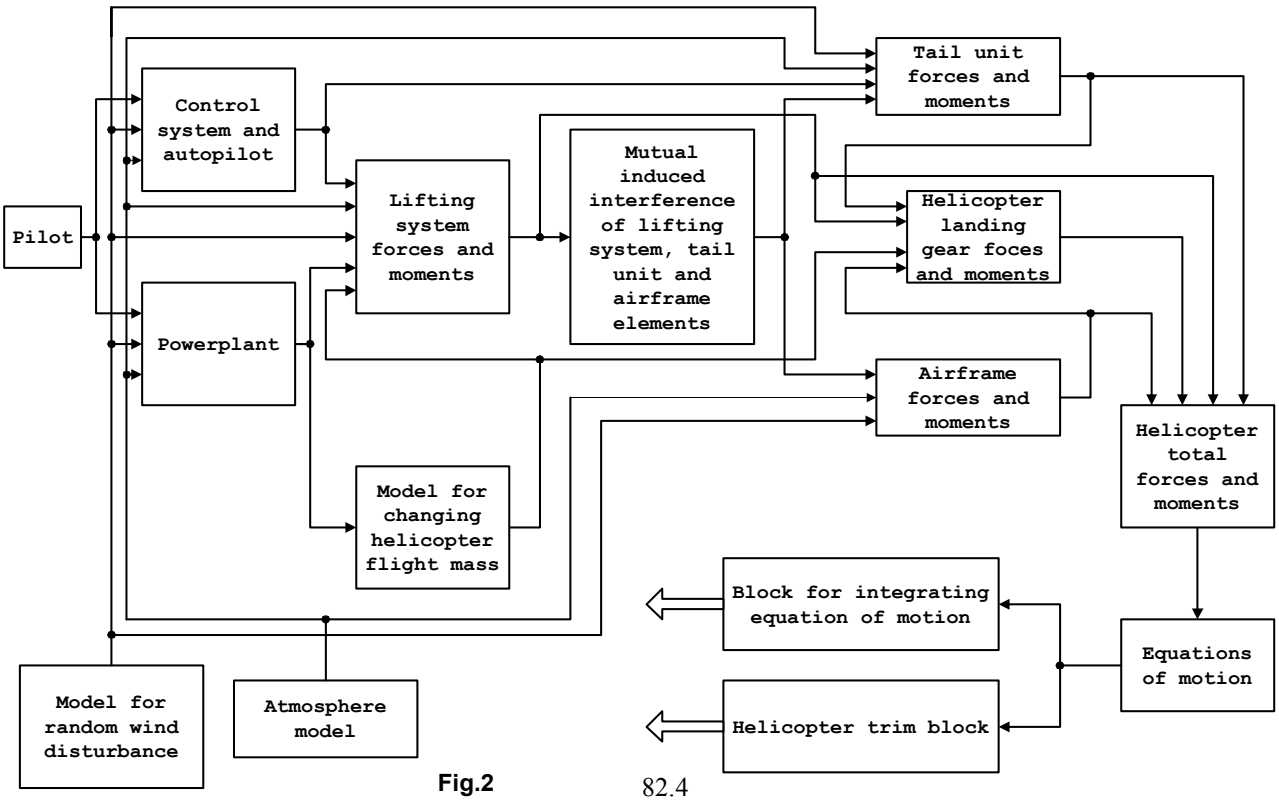

Fig.2

COAXIAL ROTOR HELICOPTER MODEL IN TSAGI WIND TUNNEL

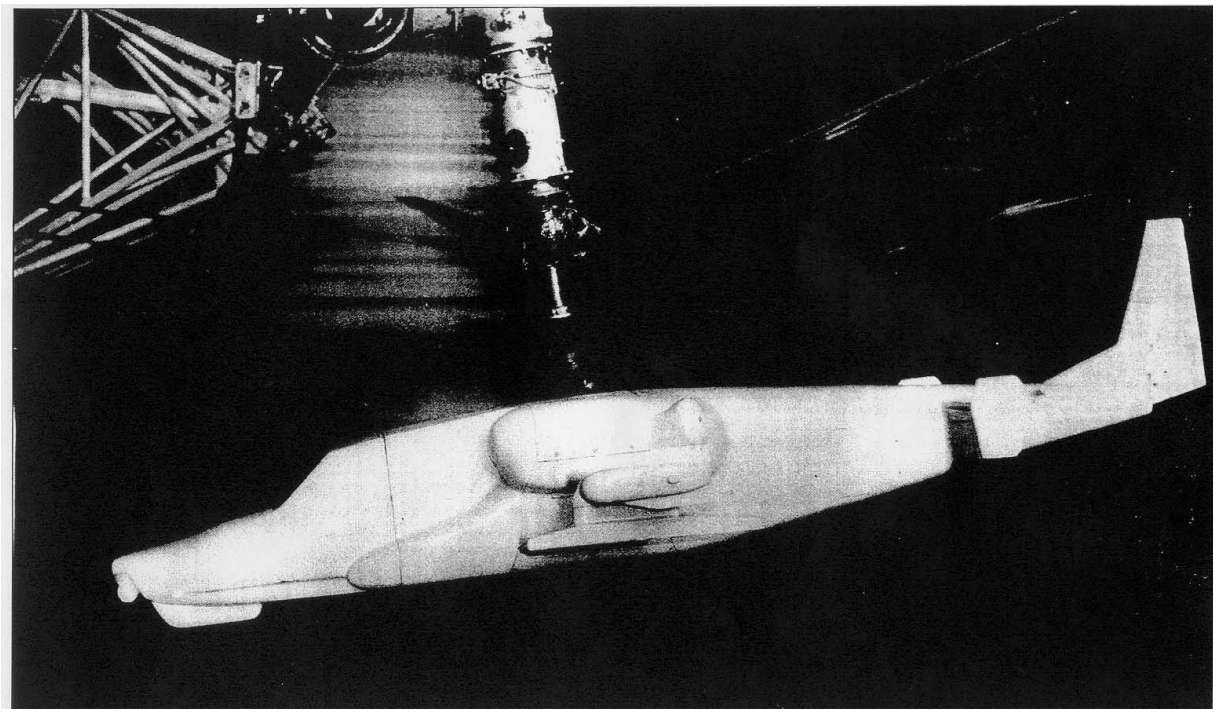

Fig. 3

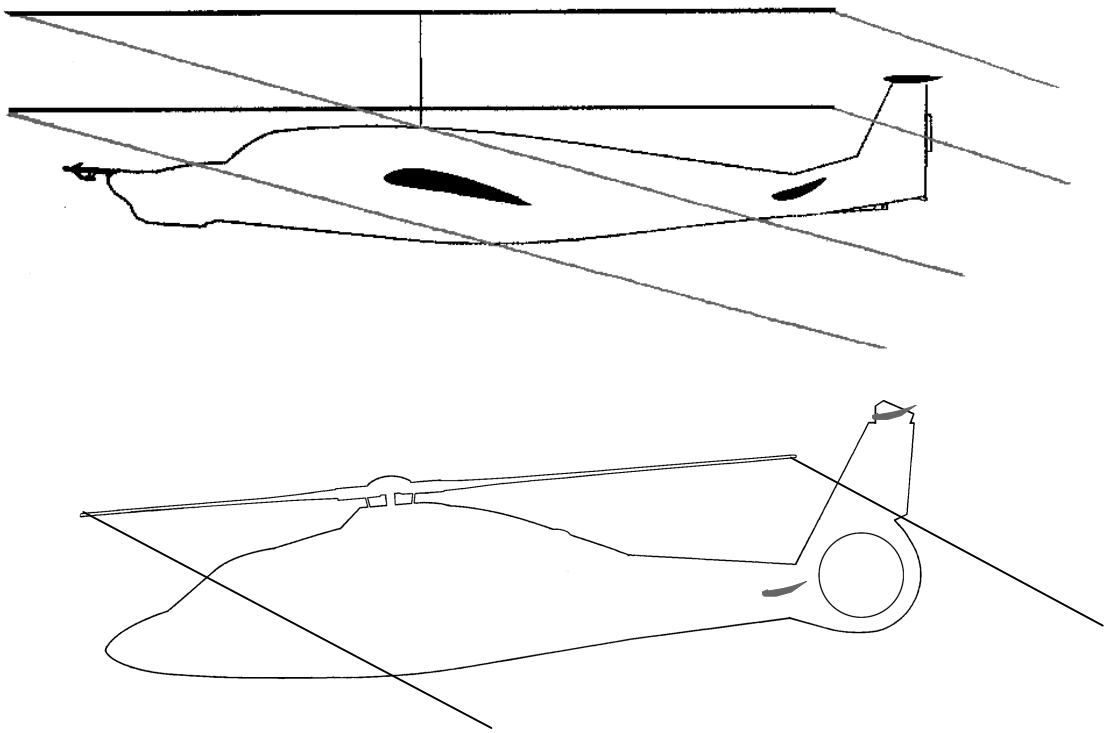

Fig. 4

Computation of velocities induced by main rotor

Computational scheme

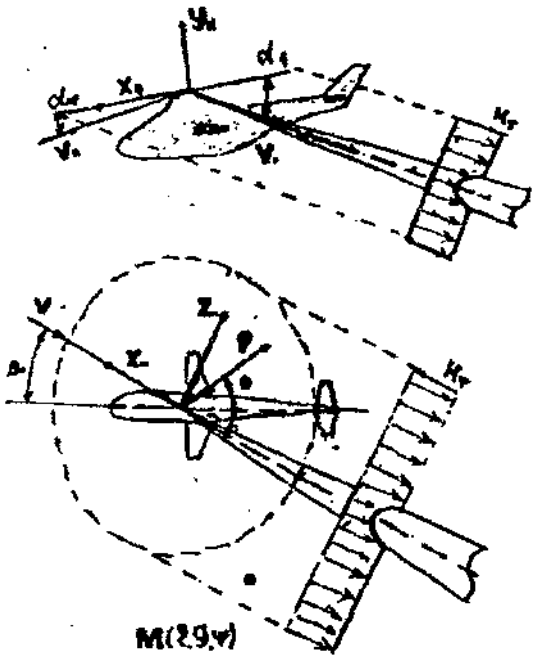

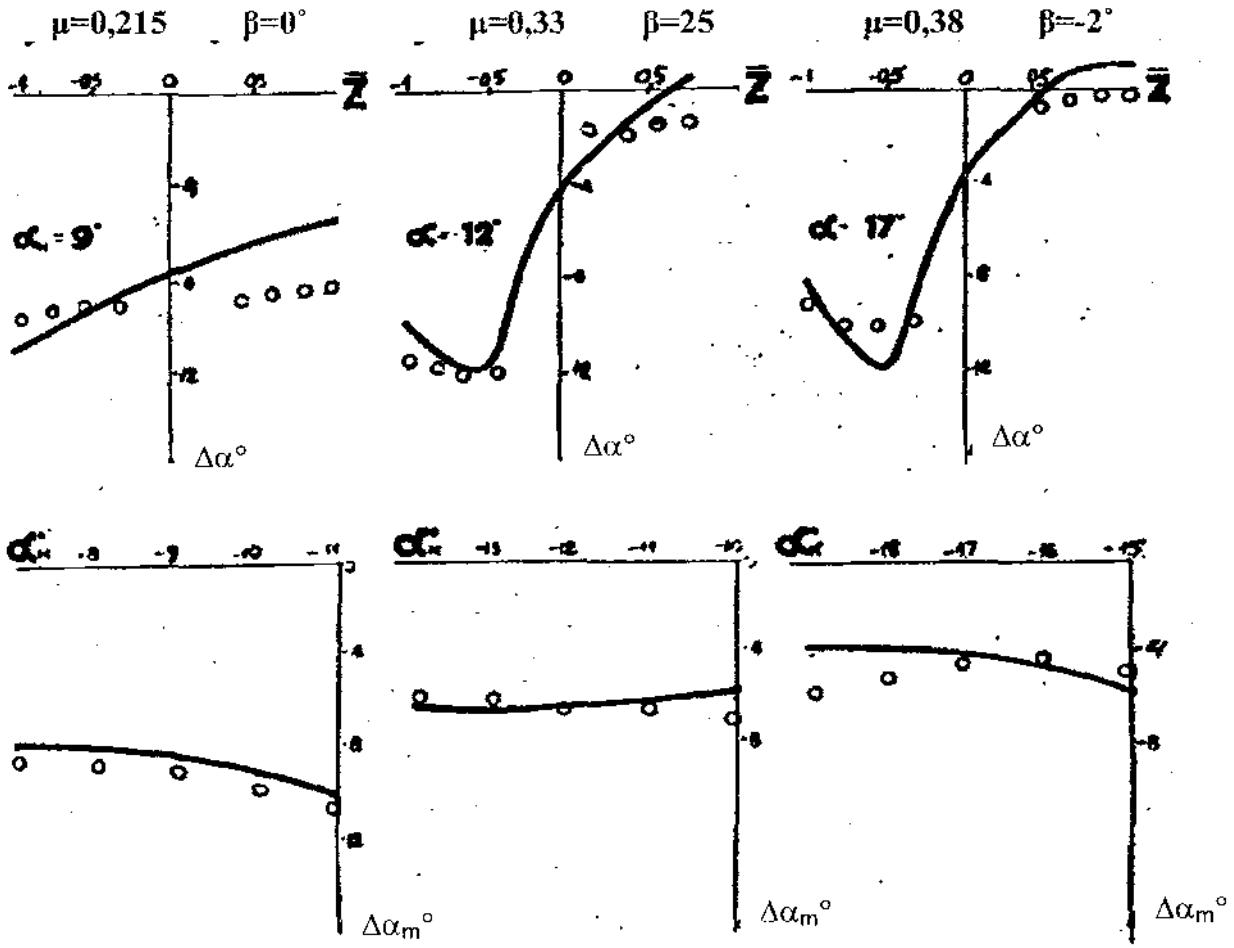

_____computation ----------experiment

Fig. 5

MATHEMATICAL MODEL OF HELICOPTER ROTOR BLADE

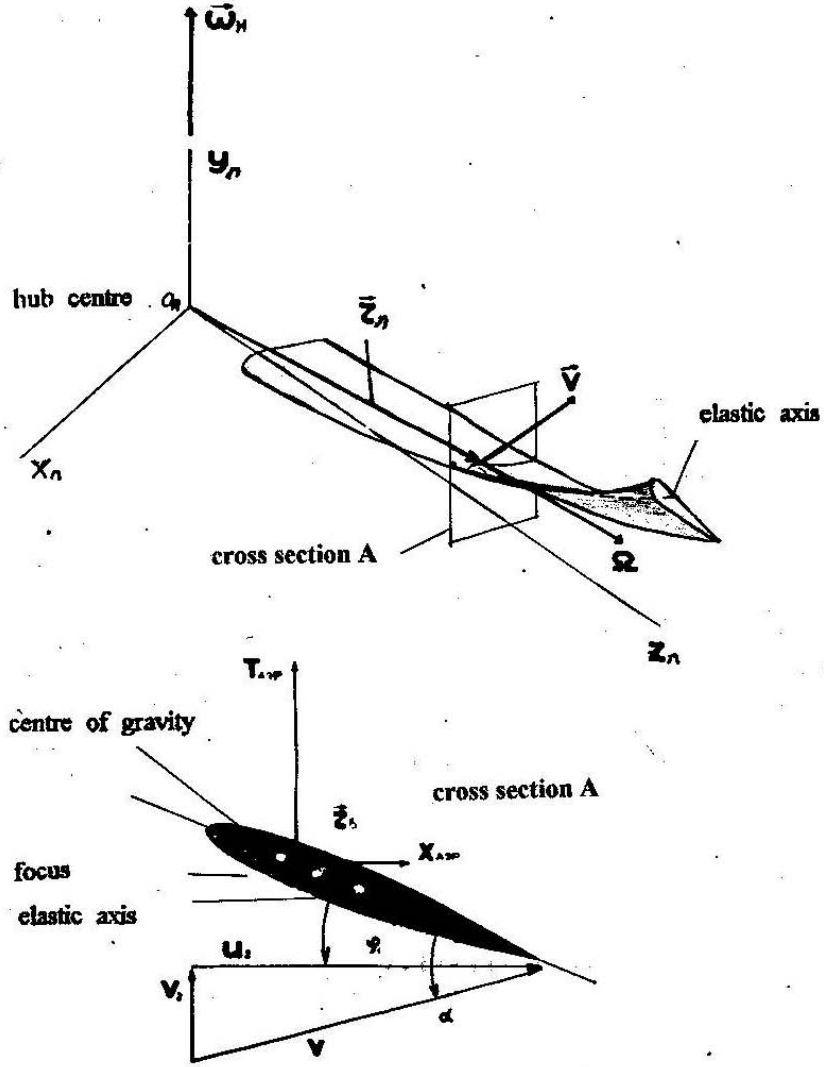

Fig. 6

Velocities and Accelerations of Blade Element

$$\vec{V}_{кэ} = \vec{V}_к + \vec{\omega} \times \vec{z}_т + (\vec{\omega} + \vec{\omega}_{мг}) \times \vec{z}_{мг} + (\vec{\omega} + \vec{\omega}_м + \vec{\omega}_н) \times \vec{z}_1 + (\vec{\omega} + \vec{\omega}_м + \vec{\omega}_н + \vec{\Omega}) \times \vec{z}_б + \vec{V}_{ос}$$

$$\vec{W}_{кэ} = \frac{d\vec{V}_{кэ}}{dt} + \vec{g}$$

System of Equilibrium Equations for Elastic Blade Element

$$\frac{\partial^2 M_x}{\partial z^2} - \frac{\partial}{\partial z}\left(\frac{\partial y}{\partial z}\int_z^R R_z\,dz\right) + \frac{\partial q_x}{\partial z} - R_x = 0$$

$$\frac{\partial^2 M_y}{\partial z^2} - \frac{\partial}{\partial z}\left(\frac{\partial x_n}{\partial z}\int_z^R R_z\,dz\right) + \frac{\partial q_y}{\partial z} - R_y = 0$$

$$\frac{\partial M_z}{\partial z} + \frac{\partial^2 x_n}{\partial z^2} M_x - \frac{\partial^2 y_1}{\partial z^2} M_y + q_z = 0$$

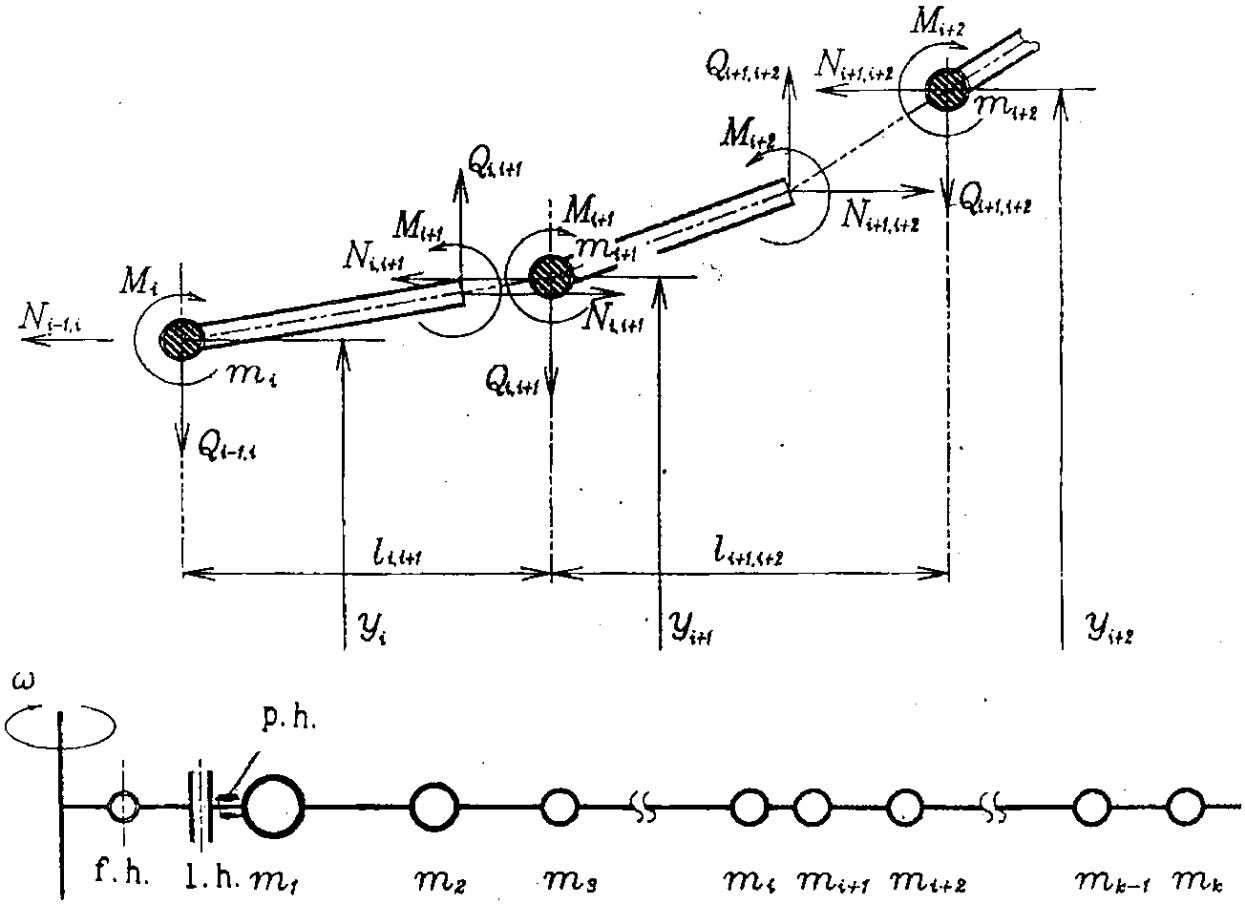
M_{i+2}
$Q_{i+1,i+2}$
$N_{i+1,i+2}$
m_{i+2}
M_{i+2}
$Q_{i,i+1}$
M_{i+1}
M_{i+1}
m_{i+1}
$N_{i+1,i+2}$
$Q_{i+1,i+2}$
M_i
$N_{i,i+1}$
$N_{i-1,i}$
$N_{i,i+1}$
m_i
$Q_{i,i+1}$
$Q_{i-1,i}$
$l_{i,i+1}$
$l_{i+1,i+2}$
y_i
y_{i+1}
y_{i+2}
ω
p. h.
f. h.
l. h.
m_1
m_2
m_3
m_i
m_{i+1}
m_{i+2}
m_{k-1}
m_k

Fig. 7

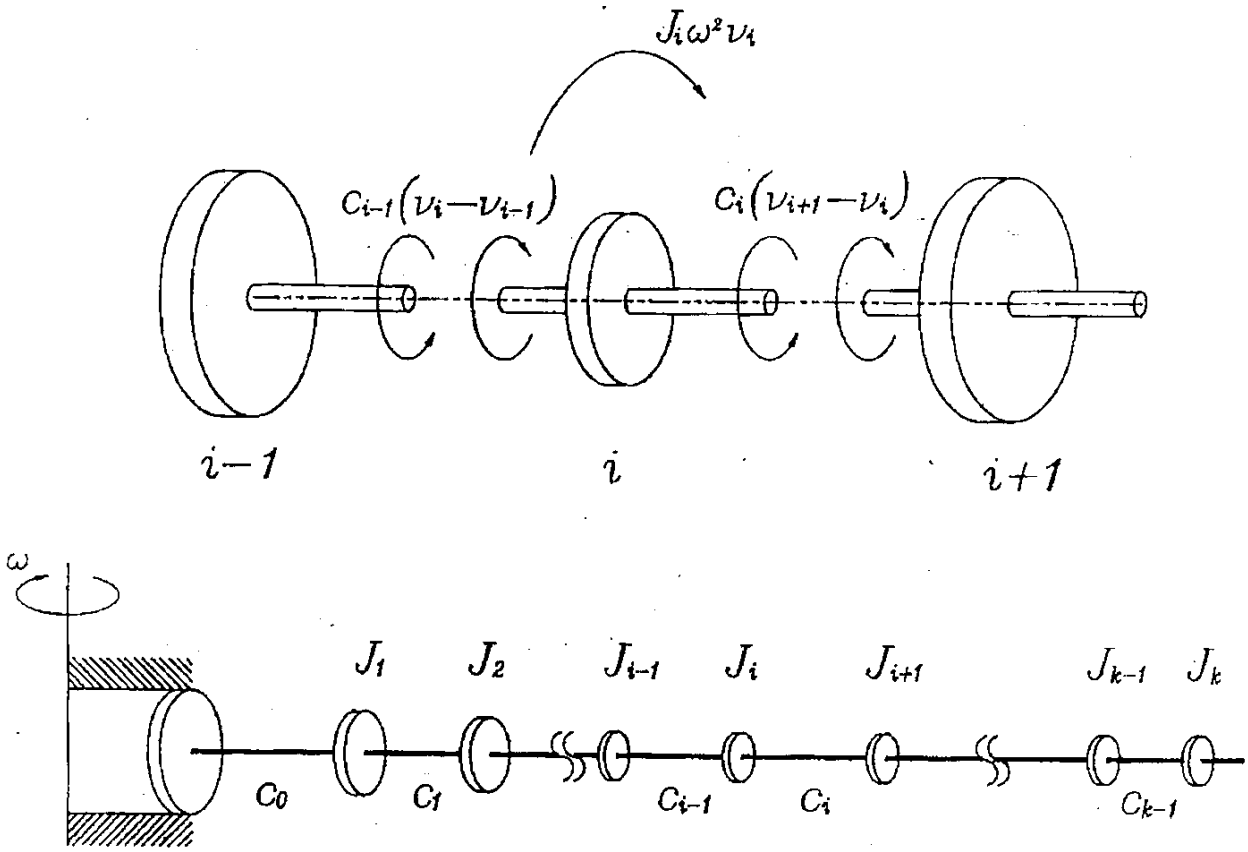
$J_i\omega^2\nu_i$
$c_{i-1}(\nu_i-\nu_{i-1})$
$c_i(\nu_{i+1}-\nu_i)$
$i-1$
i
$i+1$
ω
J_1
J_2
J_{i-1}
J_i
J_{i+1}
J_{k-1}
J_k
c_0
c_1
c_{i-1}
c_i
c_{k-1}

Fig. 8

SOLUTION OF EQUATIONS FOR BLADE MOTION

System of equations

$$m_z^k \frac{\partial^2 y_n^{nk}}{\partial t^2} - \frac{\partial^2}{\partial z^2}\left(EJ_n^k \frac{\partial^2 y_n^{nk}}{\partial z^2}\right) - \frac{\partial}{\partial z}\left(\frac{\partial y_n^{nk}}{\partial z}\int_z^R n_u^k dz\right) = F_1^{nk}$$

$$m_z^k \frac{\partial^2 x_n^{nk}}{\partial t^2} - \frac{\partial^2}{\partial z^2}\left(EJ_2^k \frac{\partial^2 x_n^{nk}}{\partial z^2}\right) - \frac{\partial}{\partial z}\left(\frac{\partial x_n^{nk}}{\partial z}\int_z^R n_u^k dz\right) - \frac{x_n^{nk}}{z} n_u^k = F_2^{nk}$$

$$J_m^k \frac{\partial^2 U_z^{nk}}{\partial t^2} - \frac{\partial}{\partial z}\left(GJ_p^k \frac{\partial U_z^{nk}}{\partial z}\right) + \omega_k^2 J_m^k U_z^{nk} = F_3^{nk}$$

n – blade number k – rotor number

Galerkin's method

$$y_n = \sum_i \delta_{Ti}(t) Y_i(z)\,;\quad x_n = \sum_j \delta_{sj}(t) X_j(z)\,;\quad U_z = \sum_z \delta_{\varphi z}(t)\Theta_z(z)$$

$i = 1.2 \ldots L \qquad j = 1.2 \ldots M \qquad z = 1.2$

$$\frac{d^2\delta_{Ti}}{dt^2} = \frac{A_i}{B_i} - \delta_{Ti} P_{Ti}^2 \;:\; \frac{d^2\delta_{sj}}{dt^2} = \frac{E_j}{G_j} - \delta_{sj} P_{sj}^2$$

$$\frac{d^2\delta_{k\varphi 1}}{dt^2} + D_1 \frac{d^2\delta_{k\varphi 2}}{dt^2} = H_1 - P_{k\varphi 1}^2 \delta_{k\varphi 1} - \omega_k^2 (\delta_{k\varphi 1} + D_1 \delta_{k\varphi 2})$$

$$\frac{d^2\delta_{k\varphi 2}}{dt^2} + D_1 \frac{d^2\delta_{k\varphi 1}}{dt^2} = H_2 - P_{k\varphi 2}^2 \delta_{k\varphi 2} - \omega_k^2 \delta_{k\varphi 1} D_1$$

Numerical Integration Method

$$\frac{d^2\delta}{dt^2} + 2f\frac{d\delta}{dt} + n^2\delta = KX + \sin\omega t$$

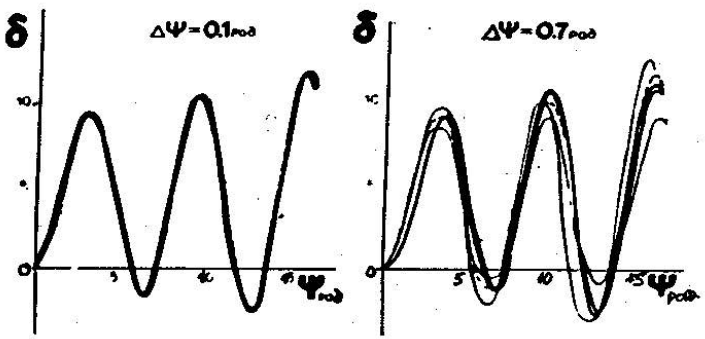

—— Analytical solution
++++ Euler's method
-+-+- Modified Euler's method
_____ Implicit method
_.-._.- Prediction-correction method

Combined Method

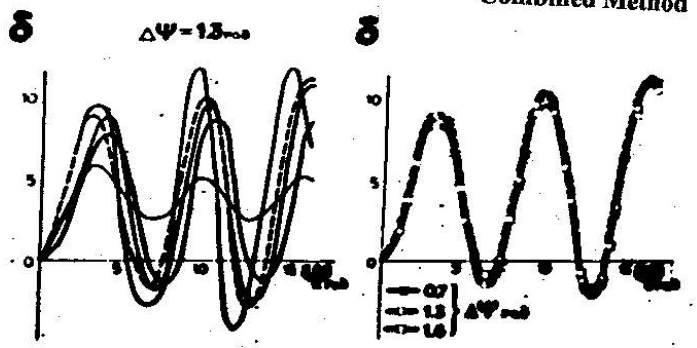

Fig. 9

Comparison with testing full-scaled main rotor in wind tunnel

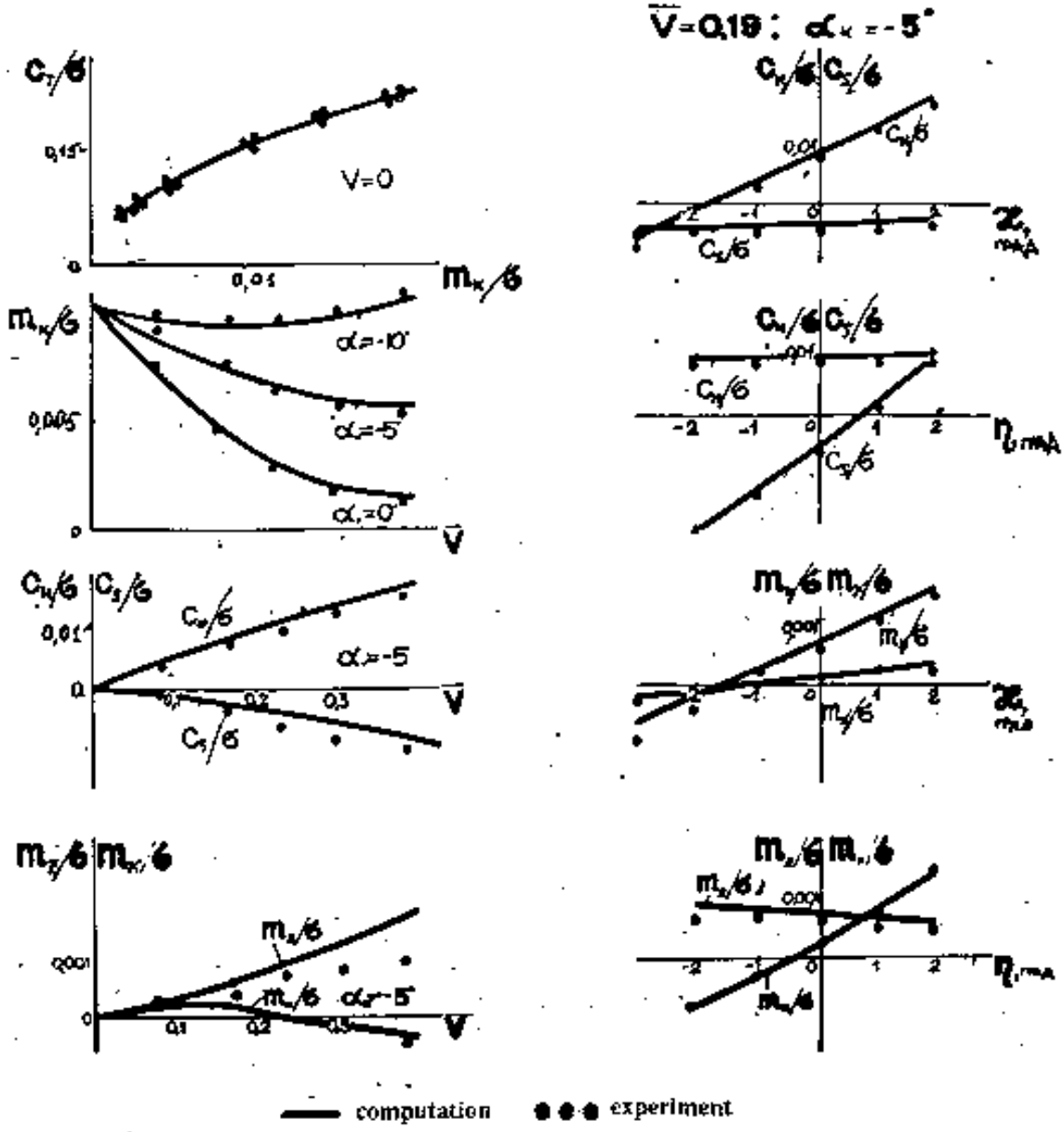

Fig. 10

TESTING HELICOPTER FULL-SCALE MAIN ROTOR IN TSAGI WIND TUNNEL

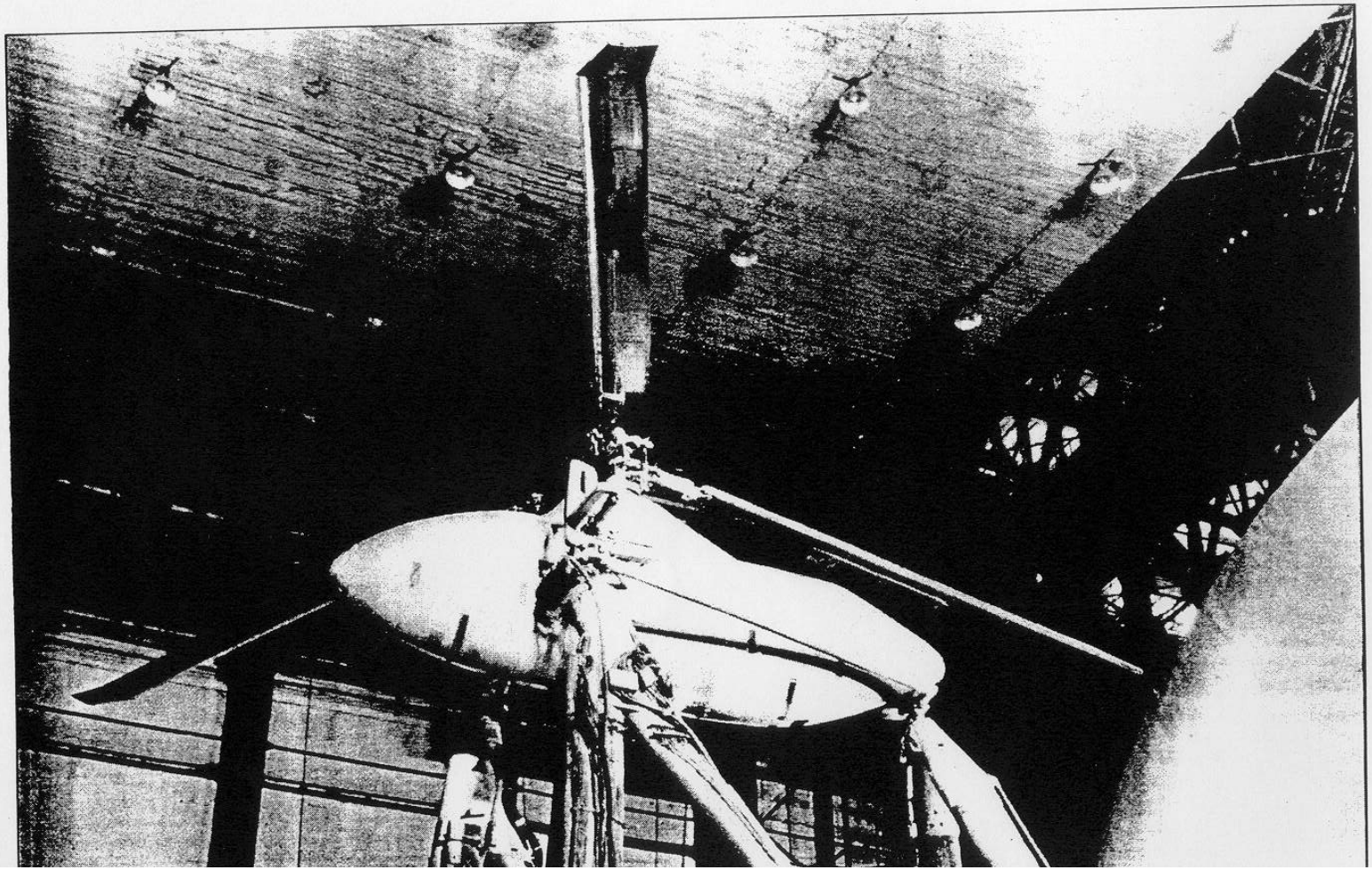

Fig. 11

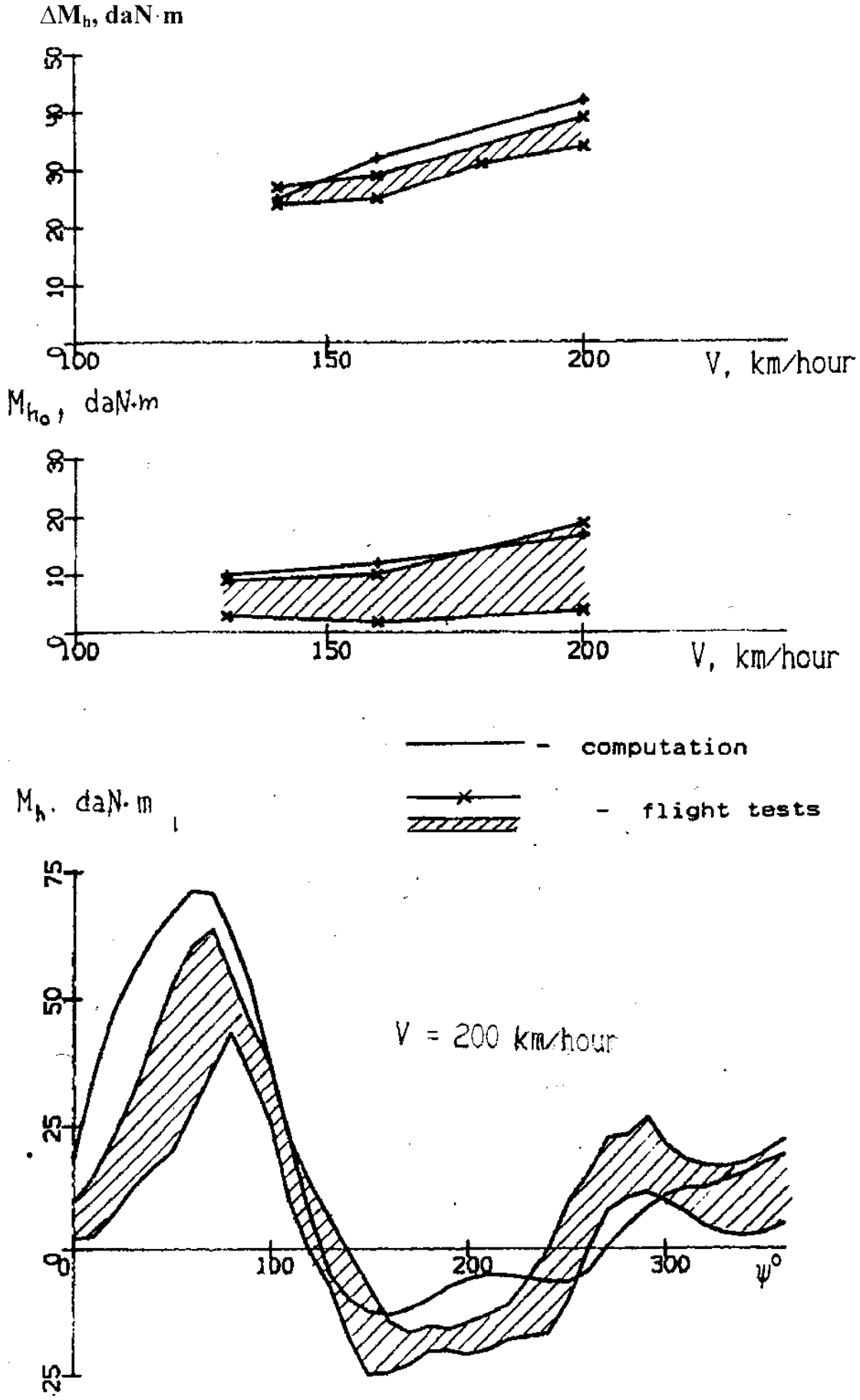
ΔMh, daN·m
50
40
30
20
10
0
100
150
200
V, km/hour
Mh0, daN·m
30
20
10
0
100
150
200
V, km/hour
- computation
- flight tests
Mh, daN·m
75
50
25
0
25
V = 200 km/hour
100
200
300
ψ°

Fig. 12

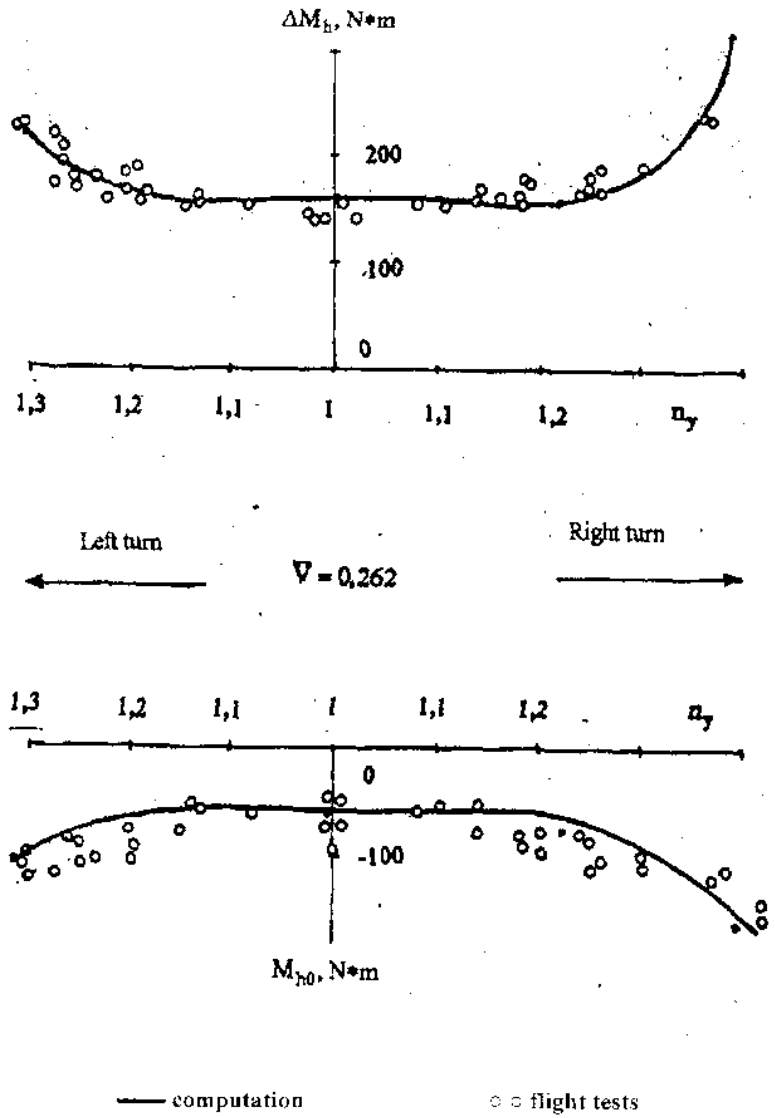
ΔM_h, N*m
200
100
0
1,3
1,2
1,1
1
1,1
1,2
n_y
Left turn
V = 0,262
Right turn
1,3
1,2
1,1
1
1,1
1,2
n_y
0
-100
M_h0, N*m
computation
flight tests

Fig. 13

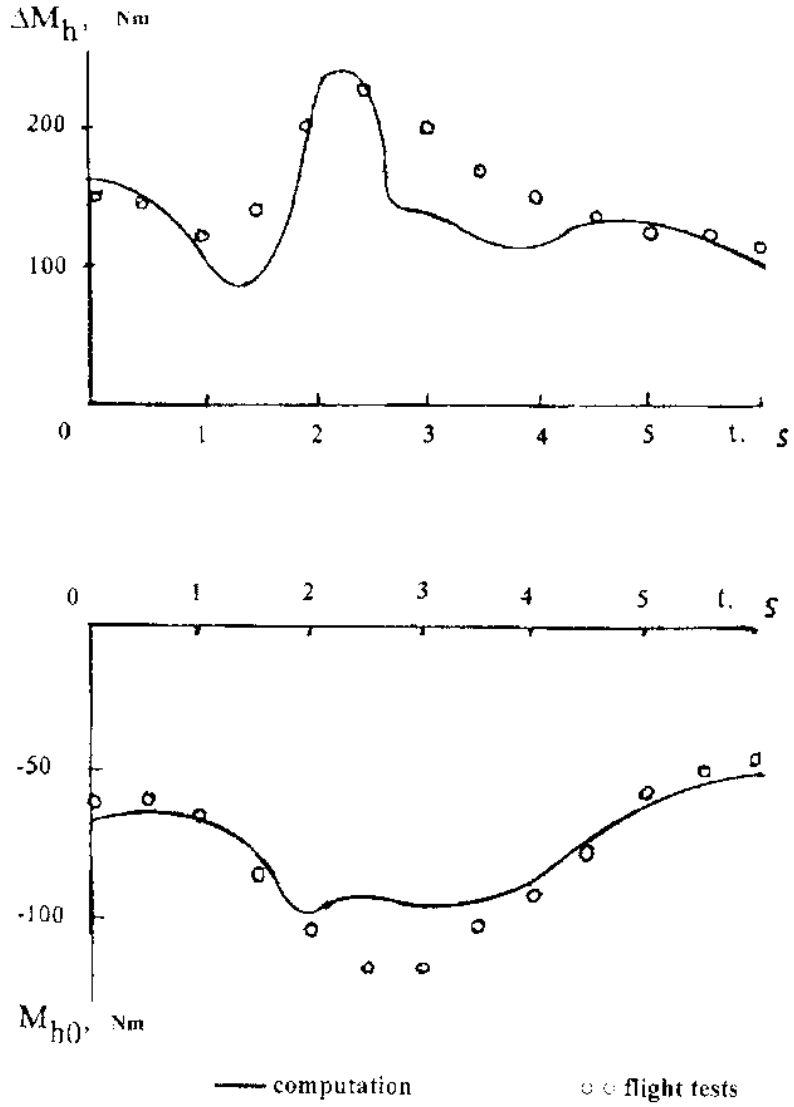
ΔM_h, Nm
200
100
0
1
2
3
4
5
t, s
0
1
2
3
4
5
t, s
-50
-100
M_h0, Nm
computation
flight tests

Fig. 14

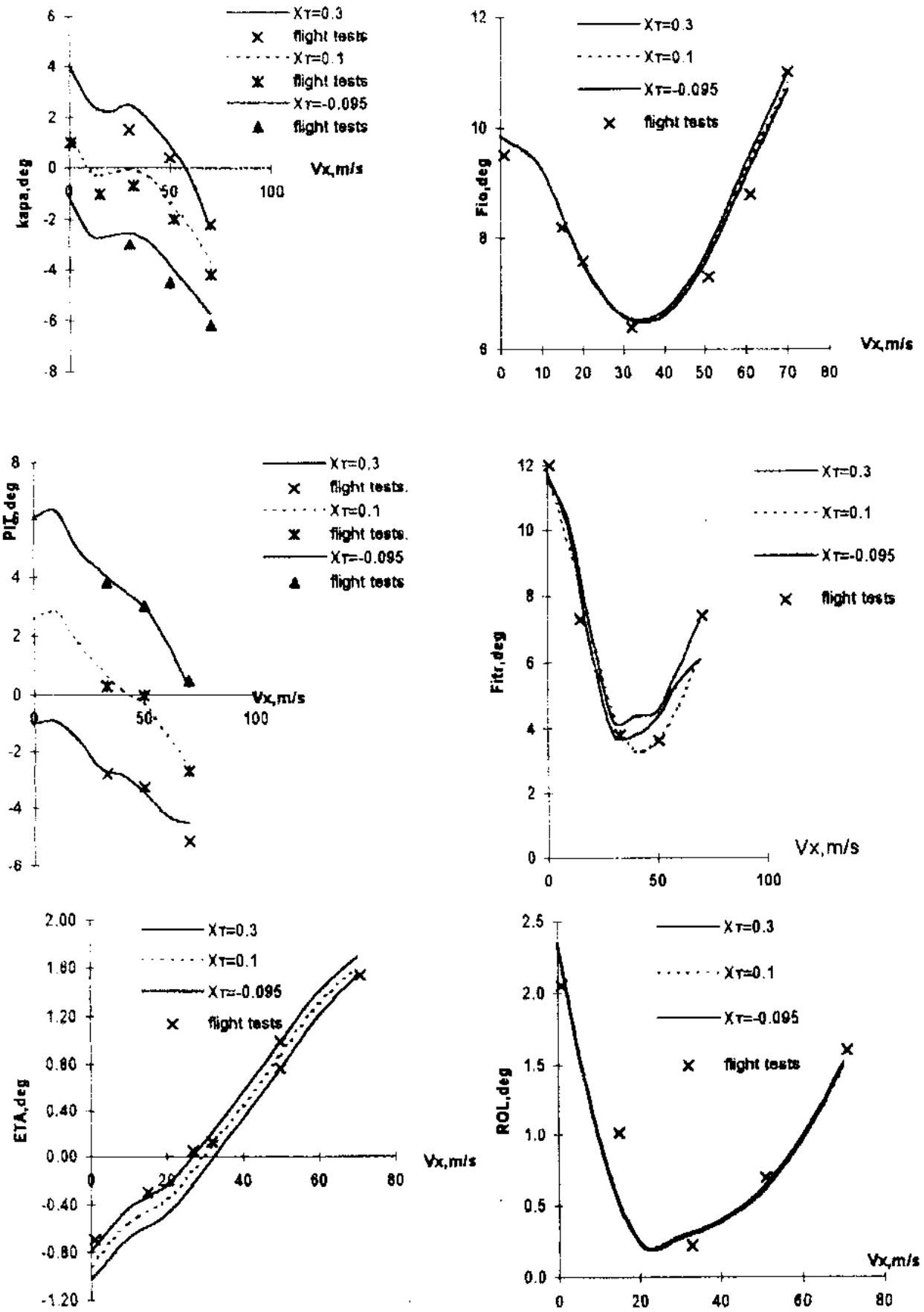

Fig. 15 Trim in level flight

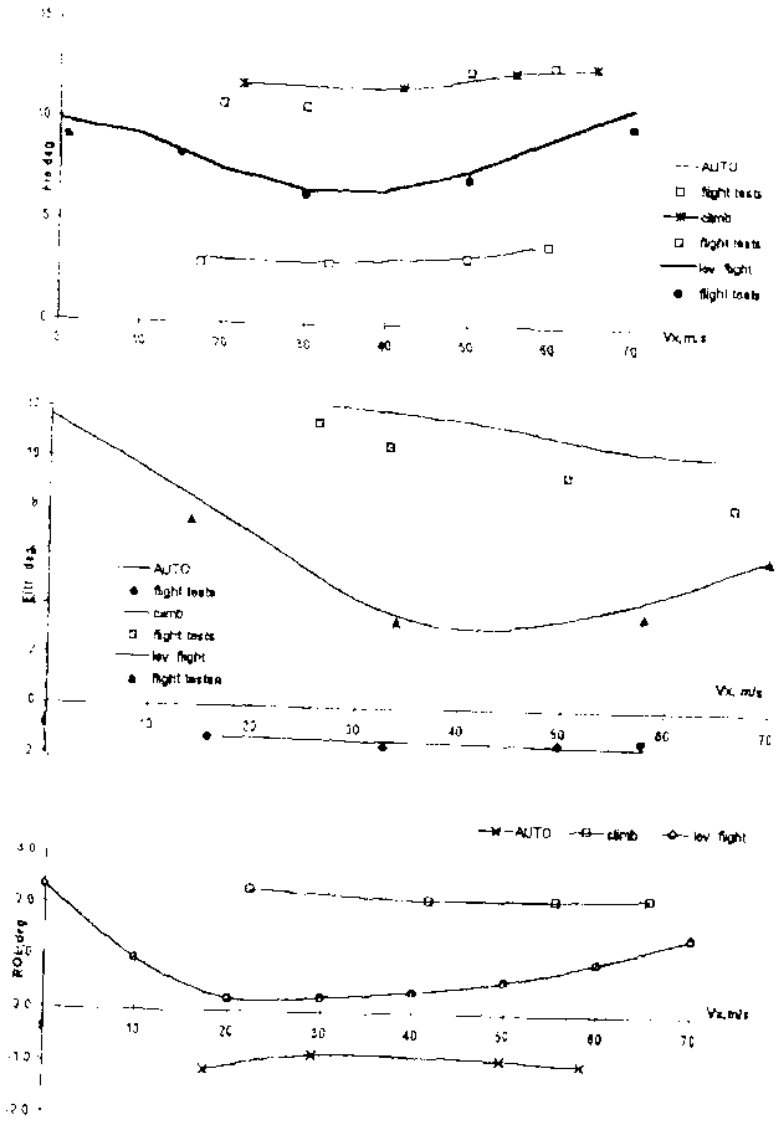

Fig. 16 Trim in level flight, in climb and autorotation

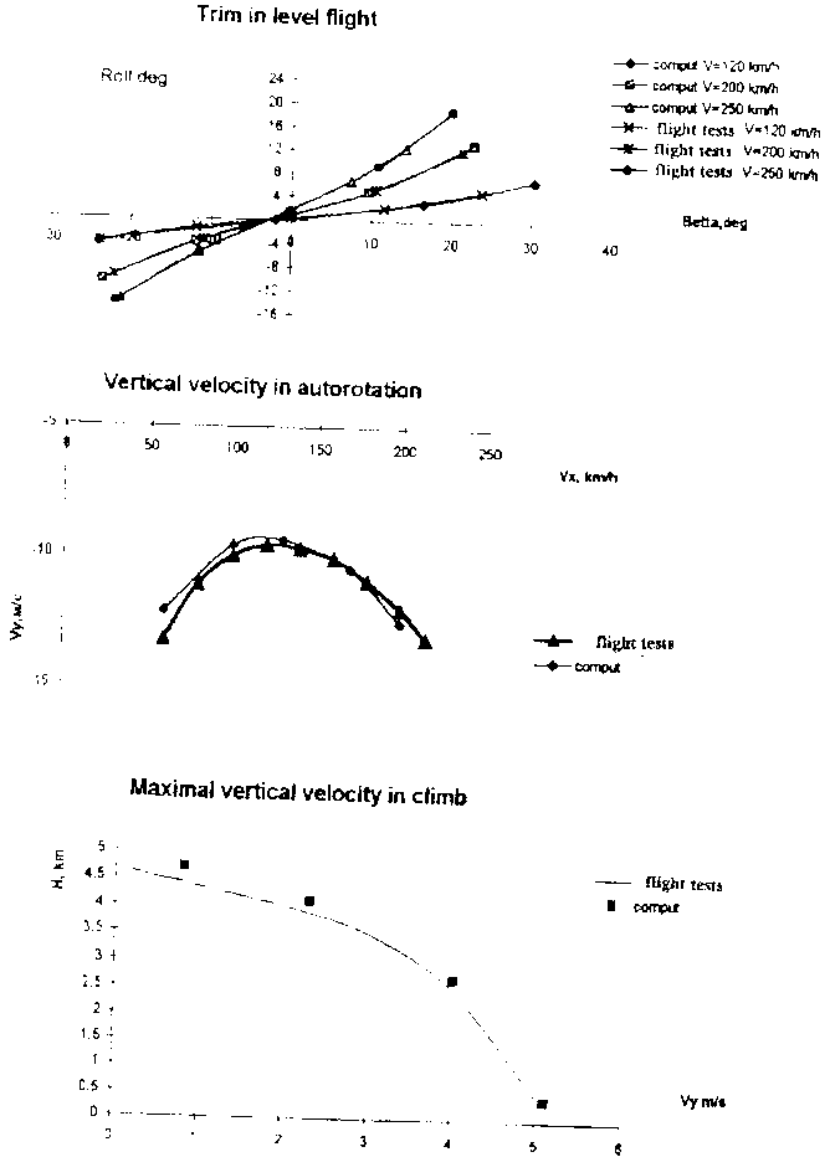

Fig. 17

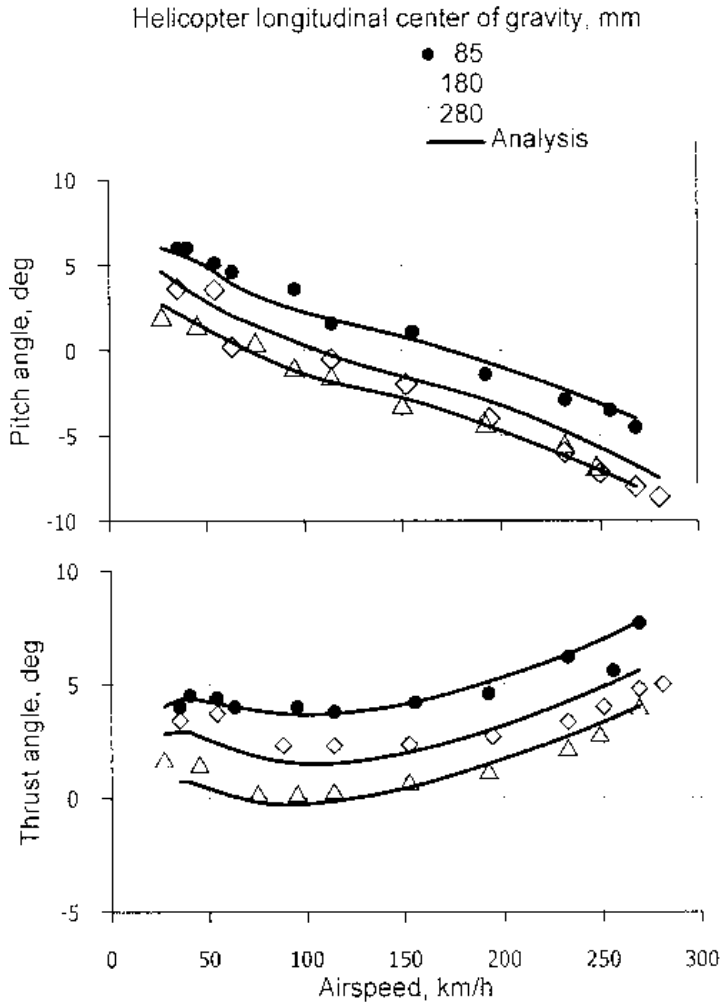

Fig. 18a Coaxial rotor longitudinal trim

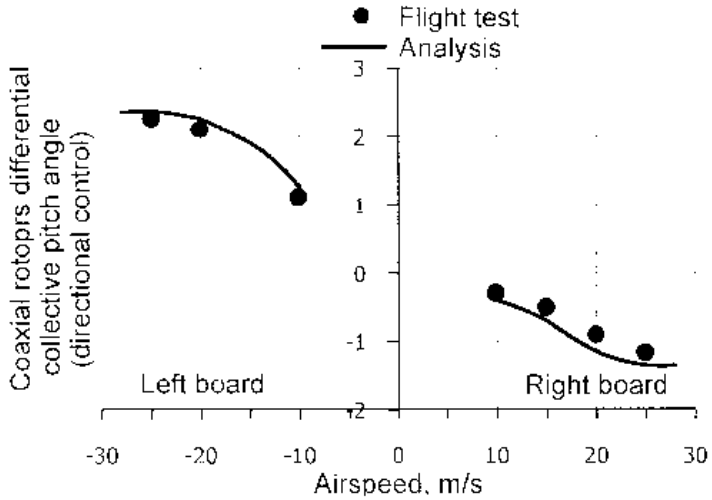

Fig. 18b Helicopter side flight

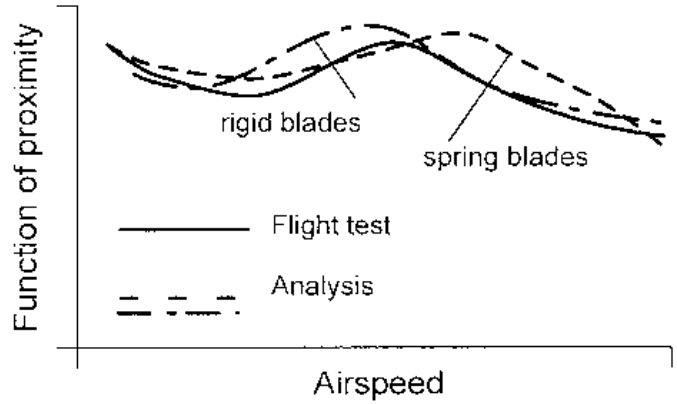

Fig. 19

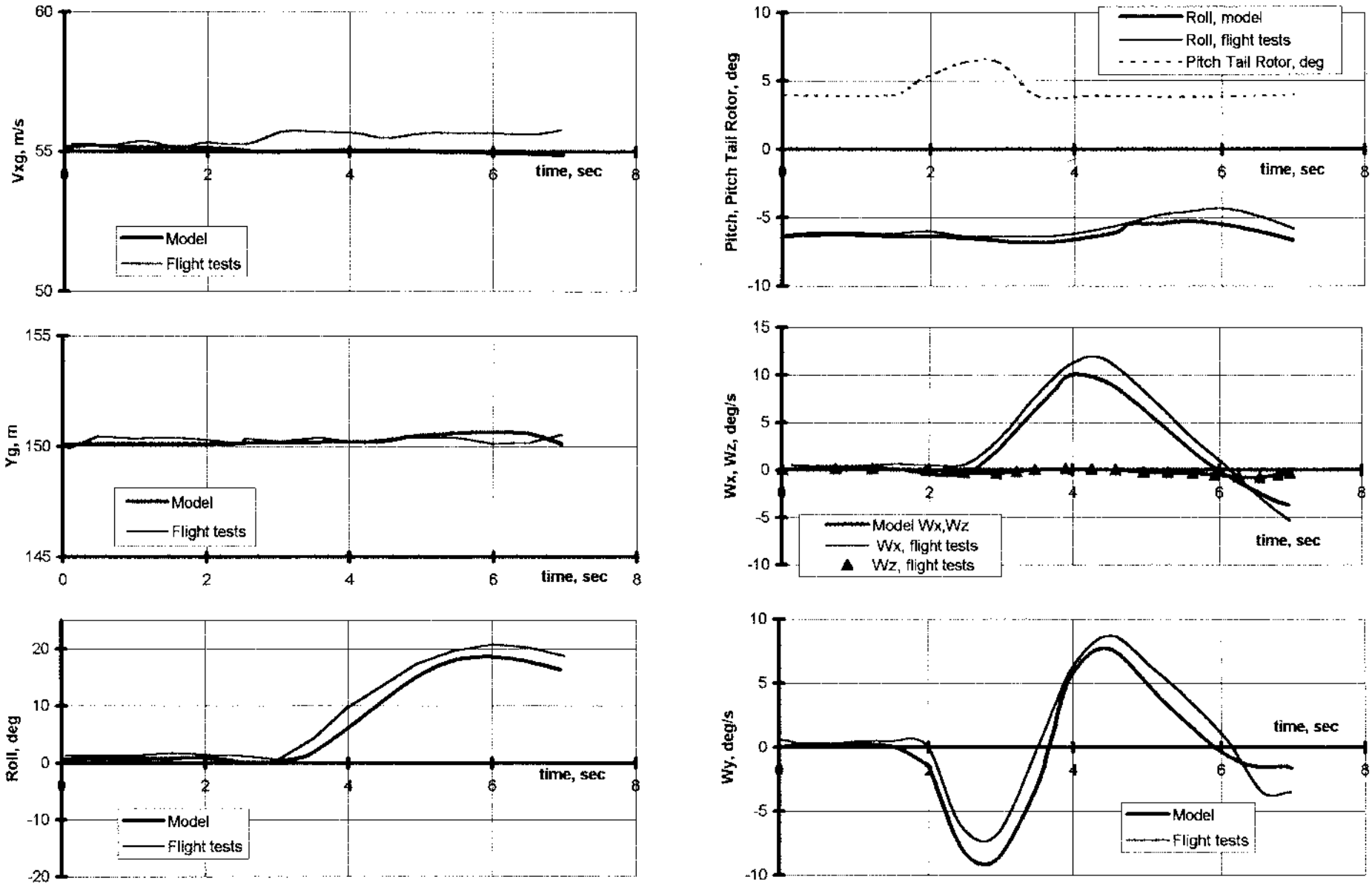

Fig. 20 Change in motion parameters when varying tail rotor pitch. Level flight, V=180 km/h

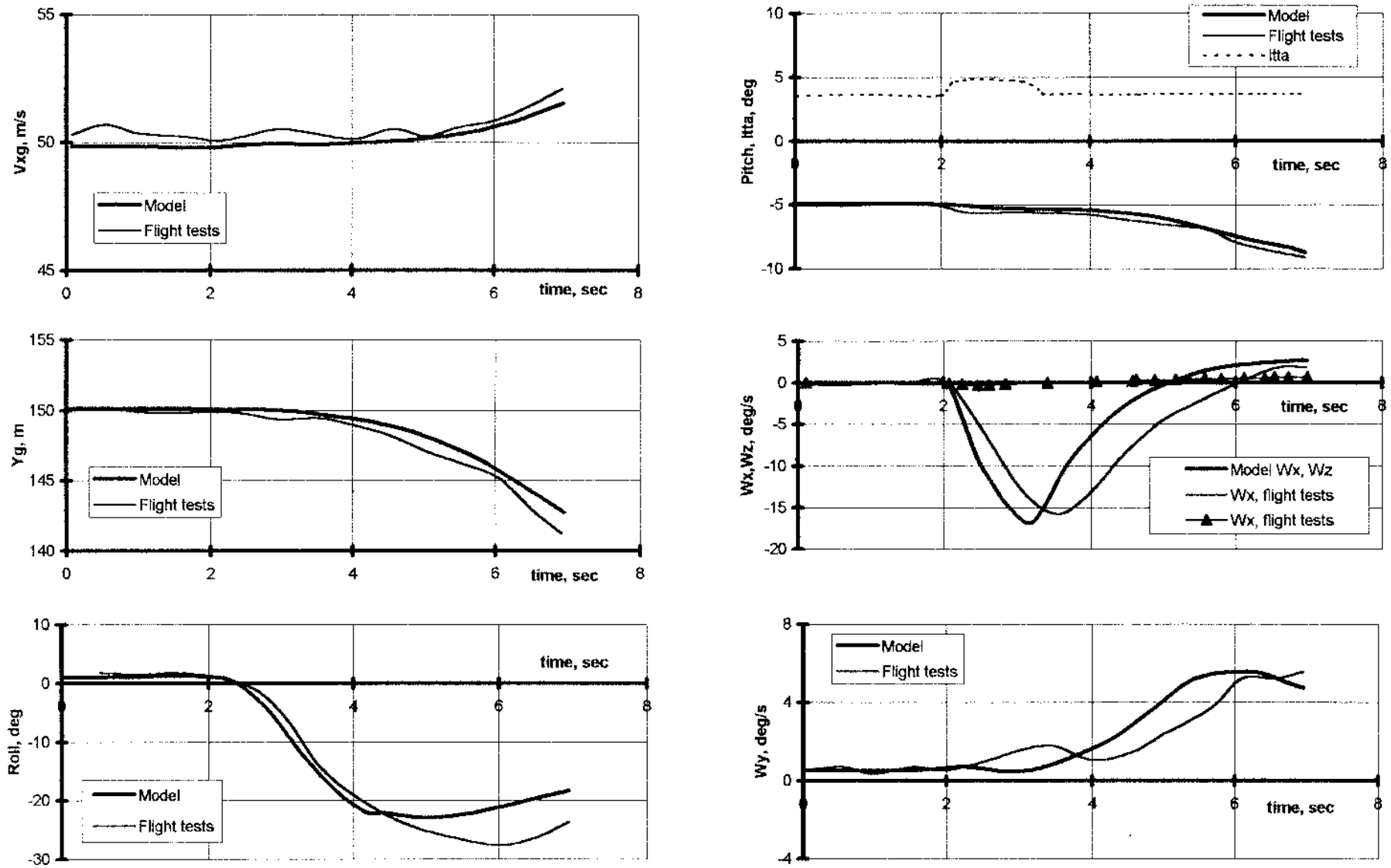

Fig. 21 Change in motion parameters with swashplate displacement in lateral plane. Level flight, V=180 km/h

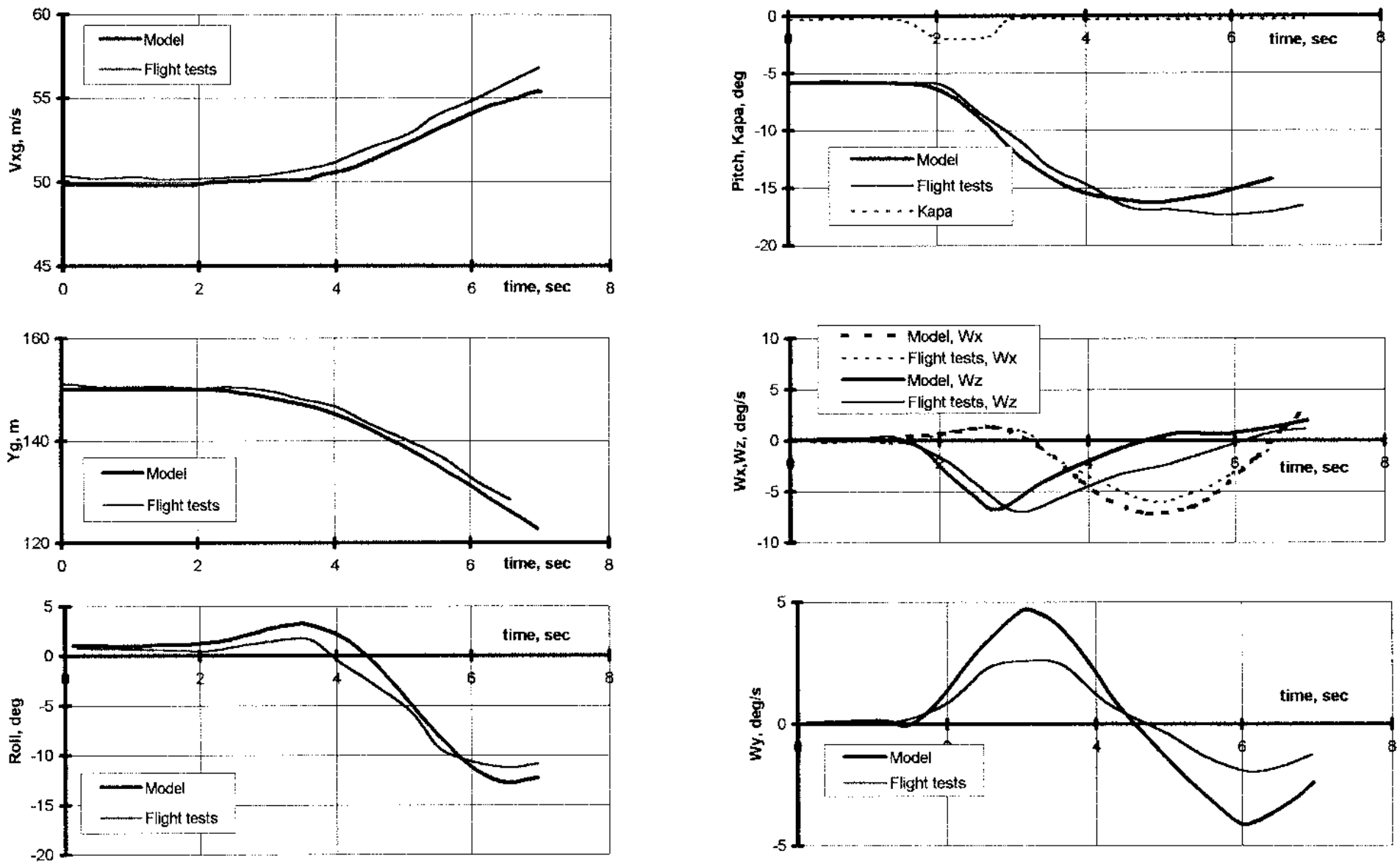

Fig. 22 Change in motion parameters with swashplate displacement in longitudinal plane. Level flight, V=180 km/h